Proceedings of ASME Turbo Expo 2013: Turbine Technical Conference and Exposition
GT2013
June 3-7, 2013, San Antonio, Texas, USA

GT2013-94341

FLUTTER PREDICTION OF A TRANSONIC FAN WITH TRAVELLING WAVE USING FULLY COUPLED FLUID/STRUCTURE INTERACTION

Hong-Sik Im *
Ge-Cheng Zha†
Dept. of Mechanical and Aerospace Engineering
University of Miami
Coral Gables, Florida 33124
E-mail: gzha@miami.edu

ABSTRACT

This paper uses a fully coupled fluid/structure interaction (FSI) to investigate the flutter mechanism of a modern transonic fan rotor with a forward travelling wave. To induce an initial travelling wave for the blade structure, an initial BC that can facilitate each blade to vibrate with a time lag by a given nodal diameter (ND) is implemented. Unsteady Reynolds-averaged Navier-Stokes (URANS) equations are solved with a system of structure modal equations in a fully coupled manner. The 5th order WENO scheme with a low diffusion E-CUSP Riemann solver is used for the inviscid fluxes and a 2nd order central differencing is used for the viscous terms. A half annulus sector is used for the flutter simulations with a time shifted phase lag boundary condition at the circumferential boundaries. The present FSI simulations show that the shock instability causes the flutter. When the detached normal shock moves further upstream in a direction normal to the blade chord, the interaction of the detached normal shock with tip leakage vortex creates more serious blockage to the blade passage that can introduce an aerodynamic instability to the blade structure due to the incoming flow disturbance, resulting in flutter. The flutter of the transonic fan observed in this study occurs at the 1st mode before the stall. The predicted flutter boundary agrees well with the experiment.

1 Introduction

Flutter of turbomachinery is a fluid/structure interaction instability of a deformable blade structure with surrounding fluid flow. If vibration induced by aerodynamic force acting on the blade structure exceeds a condition of dynamic equilibrium, the blade flutter occurs at/near a blade natural frequency [1–3].

In aircraft engine fans/compressors, flutter may occur in several ways including subsonic/supersonic stall flutter, supersonic unstalled flutter, choking flutter and acoustic flutter. Recent studies [4–9] have demonstrated the importance of the unstalled supersonic flutter. Unlike stall flutter, the supersonic flutter occurs at a stable operation and there are no such remedies to cure the supersonic flutter because it often involves extremely complex fluid flow instabilities such as shock unsteadiness, shock/boundary layer interaction, and shock/vortex interaction. For example, unsteady shock oscillation rather than blade stall were found to be the driving mechanism for flutter instability in a transonic fan [5]. The shock location and movement and its relation to the inter blade phase angle contributes significantly to the variation in the aerodynamic damping [6]. The comparison with measured data for the onset of a transonic fan flutter by Chew et al. [7] shows that the shock movement of the blade passage appears an important parameter causing the fan flutter due to the interaction of the passage shocks with the suction surface boundary layer. Vahdati et al. [8] shows that the flow separation behind the shock on the suction surface is the key driver of a wide-chord transonic fan flutter. Another study showed that shock has both stabilizing and destabilizing effect with the inter-blade phase angle and location of shock having a significant impact on stability [9]. As presented in this paper, the detached normal shock unsteadiness associated with the tip leakage vortex and with the suction surface boundary layer appears the root cause of the highly loaded transonic

*ASME Member, Ph.D., Currently an engineer at Honeywell
†Associate Professor, ASME Fellow

fan flutter observed in this study.

To achieve accurate solutions of these highly nonlinear fluid/structural instabilities during the fan/compresror flutter, the governing equations of structural and fluid motion have to be simultaneously solved. However, many of fluid-structural interaction (FSI) simulations are implemented by a loosely coupled or non-fully coupled procedure, i.e the structural response lags behind the flow solver by one or a few time steps since the information is exchanged after partial or complete convergence of individual solvers [10]. For example, Gnesin et al. [11] solved the unsteady Euler equations with the modal approach for the structure analysis in the partially coupled manner. Doi et al. [12] loosely coupled an explicit Runge-Kutta multigrid flow solver with a FEM structure solver to predict the aeroelastic forced responses of NASA Rotor 67 blade. In the work of Carstens et al. [13] and Sayma et al. [14], the structural part of the governing equations is time-integrated using Newmark scheme, while the unsteady airloads are computed at every time step by a Navier-Stokes code. Chew et al. [7] used inviscid linearized model, in which the flow governing equations are linearized by considering the flow unsteadiness to be small, to capture stall flutter (or referred to as part-speed flutter) of a civil wide chord fan and a low aspect ratio military fan engine. Due to some shortcomings such as neglecting viscous terms, endwall boundary layers and tip clearance, their computation fails to show any signs of flutter instability, which was observed in the testing. It is also shown that the conventional energy method, in which the blade vibration and aerodynamic forces may be treated independently, could not accurately capture the modern fan flutter boundary while the coupled mode flutter analysis methods do [15].

In the work of Im et al. [16], the fully coupled FSI [17] developed by Chen et al. [17] is further extended for turbomachinery by implementing an advanced blade tip deforming mesh generation technique to capture the transonic rotor flutter. In the fully coupled FSI [17], the governing equations of structural and fluid motion are simultaneously solved by exchanging the unsteady aerodynamic force and structural displacement within each physical time step via a successive iteration on the pseudo-time step. The fully coupled FSI methodology adopted in this study is shown to accurately predict the supersonic flutter boundary of the 3D wing associated with the strong shock/boundary layer interaction [18].

The purpose of this paper is to investigate the mechanism behind a modern transonic fan flutter with a forward travelling wave using the fully coupled fluid/strcuture interaction [16]. The half annulus sector is used with the time shifted phase lag BC [19] at the circumferential boundaries. Since flutter of transonic fans often involves a travelling wave [20, 21], in which the blades vibrate at the same frequency but with a constant phase difference, in this paper a travelling wave BC that can facilitate each blade to vibrate with a time lag is implemented. Note if the phase difference propagates in the same direction to the rotor rotation, it is called forward travelling wave(FTW). If the phase difference propagates in the opposite direction to the rotor rotation, it is called backward travelling wave(BTW).

Nomenclature

b_s	blade root semi-chord
C_p	pressure coefficient, $\frac{2(p-p_\infty)}{\rho_\infty U_\infty^2}$
$\mathbf{F}$	total aerodynamic force
L_∞	blade chord at hub
N_B	number of blade
N_D	nodal diameter
U_∞	absolute velocity at inlet
$\frac{\Delta S}{R}$	change of entropy, $\frac{\gamma}{\gamma-1} ln \frac{To}{To_\infty} - ln \frac{Po}{Po_\infty}$
ρ_∞	fluid density at inlet
φ	inter blade phase angle (IBPA)
$\bar{m}$	blade mass
$\bar{V}$	frustum volume
V^*	reduced velocity, $\frac{U_\infty}{b_s \omega_\alpha}$
V_f	flutter speed index, $\frac{V^*}{\bar{\mu}}$
ω_α	1st torsional mode natural frequency
$\bar{\mu}$	mass ratio, $\frac{\bar{m}}{\bar{V}\rho_\infty}$
- Abbreviations -	
BC	Boundary Condition
FSI	Fluid/Structure Interaction
FTW	Forward Travelling Wave
$CUSP$	Convective Upwind and Splitting Pressure
$URANS$	Unsteady Reynolds-averaged Navier-Stokes
$WENO$	Weighted Essentially Non-oscillatory

2 Aerodynamic Model

Since a fewer number of modes are usually enough to predict the fan flutter in the coupled mode approach [15], time accurate 3D compressible Navier-Stokes equations with the Spalart-Allmaras (S-A) model [22] in a rotating frame [23] are solved with a system of 5 decoupled modal equations in a fully coupled manner in this study. The Low Diffusion E-CUSP (LDE) Scheme [24] as an accurate shock capturing Riemann solver is used with a 5th order WENO scheme for inviscid flux and a 2nd order central differencing for viscous terms [25] in order to resolve such complex shock related instabilities during the flutter. An implicit 2nd order dual time stepping method [26] is solved using an unfactored Gauss-Seidel line iteration to achieve high convergence rate. The high-scalability parallel computing is implemented to save wall clock time [27].

3 Structural Model

Since the stiffness of the rotor disk is much larger than that of the compressor blades, the rotor disk vibration is neglected. The equation of motion of an N-DOF(degree of freedom) system with the mechanical damping and the aerodynamic loading as the excitation force can be presented in matrix form:

$$[\mathbf{M}]\{\ddot{\mathbf{X}}\} + [\mathbf{C}]\{\dot{\mathbf{X}}\} + [\mathbf{K}]\{\mathbf{X}\} = \{\mathbf{F}\} \tag{1}$$

where, **M**, **C**, **K** are the mass, structural damping and stiffness matrices. Due to the damping matrix **C**, above Eq. (1) is

generally a set of N coupled equations. **F** as given in Eq. (2) is the total aerodynamic force and is obtained by eliminating the static load from the converged RANS solutions such that the blade vibration can have the equilibrium position of around zero.

$$\mathbf{F} = -\oint P \cdot \hat{n} dA + \oint \tau_{\mathbf{w}} \cdot \hat{t} dA \tag{2}$$

where, $\hat{n}$ is the unit normal vector to the blade surface and $\hat{t}$ is the unit tangent vector to the blade surface. P is the fluid static pressure and $\tau_{\mathbf{w}}$ is the fluid wall shear stress acting on the blade surface. It is shown by Gruber and Carstens [28] that viscous effects can cause a significant difference in aerodynamic damping.

3.1 Decoupled Modal Equations

To decouple the equations of motion for the damped systems(1), we use the mass normalized mode shape($\tilde{\phi}$) defined as the normal modes divided by square root of the generalized mass($\sqrt{\phi^T m \phi}$). Let

$$\{\mathbf{X}\} = [\tilde{\Phi}]\{\mathbf{q}\} \tag{3}$$

and premultiply Eq. (1) by the transpose $[\tilde{\Phi}]^T$.

$$\begin{aligned}[\tilde{\Phi}]^T[\mathbf{M}][\tilde{\Phi}]\{\ddot{\mathbf{q}}\} + [\tilde{\Phi}]^T[\mathbf{C}][\tilde{\Phi}]\{\dot{\mathbf{q}}\} + [\tilde{\Phi}]^T[\mathbf{K}][\tilde{\Phi}]\{\mathbf{q}\} \\ = [\tilde{\Phi}]^T\{\mathbf{F}\}\end{aligned} \tag{4}$$

where **q** is the vector of the principal coordinates.

Using the orthogonality of the system matrices and assuming damping matrix to be a linear combination of the mass and stiffness matrices, Eq. (4) is then completely decoupled and the *j*th equation will have the form

$$\ddot{q}_j + 2\zeta_j \omega_j \dot{q}_j + \omega_j^2 q_j = \frac{\tilde{\phi}_j^T}{m_j}\mathbf{F} \tag{5}$$

where $[\tilde{\Phi}]^T = [\tilde{\phi}_1, \cdots, \tilde{\phi}, \cdots, \tilde{\phi}_N]^T$. N is the number of modal coordinates. ω_j and ζ_j are natural frequency and modal damping ratio for mode j. m_j denotes the jth diagonal element of modal mass matrix which will be unity. In the current study, the structural system may be reduced to only five mode shapes, since a few bending and torsional frequencies are usually sufficient to determine flutter. The normalized modal equation can be given as [17, 29]

$$\ddot{q}_j + 2\zeta_j(\frac{\omega_j}{\omega_\alpha})\dot{q}_j + (\frac{\omega_j}{\omega_\alpha})^2 q_j = \frac{\tilde{\phi}_j^{*T}}{m_j^*} \cdot \mathbf{F}^* \cdot {V_f}^2 \cdot \frac{b_s^2 L_\infty}{\bar{V}} \cdot \bar{m} \tag{6}$$

where the dimensionless quantities are denoted by an asterisk. $V_f(= \frac{U_\infty}{b_s \omega_\alpha \sqrt{\bar{\mu}}})$ is the flutter speed index which is an input flutter control parameter. $\bar{m}$ is the measured blade mass, $\bar{V}$ represents the conical frustum volume and b_s is the streamwise root semi chord. L_∞ is the reference length and ω_α is the angular frequency of the first torsional mode in units *radians*/*sec*. $\bar{\mu}(= \frac{\bar{m}}{\bar{V}\rho_\infty})$ stands for the mass ratio, i.e. the ratio between the structural mass and the mass of the equivalent volume of fluid at reference density. It is noticed that m_j^* should be equal to one when the mass normalized mode shapes are used.

The equations are then transformed to a state form as follows:

$$[\widetilde{\mathbf{M}}]\frac{\partial \mathbf{S}}{\partial t} + [\widetilde{\mathbf{K}}]\{\mathbf{S}\} = \mathbf{q} \tag{7}$$

where

$$\mathbf{S} = \begin{pmatrix} q_j \\ \dot{q}_j \end{pmatrix}, \widetilde{\mathbf{M}} = [I], \widetilde{\mathbf{K}} = \begin{pmatrix} 0 & -1 \\ (\frac{\omega_j}{\omega_\alpha})^2 & 2\zeta_j(\frac{\omega_j}{\omega_\alpha}) \end{pmatrix}$$

$$\mathbf{q} = \begin{pmatrix} 0 \\ \phi_j^{*T} \cdot \mathbf{F}^* \cdot V_f \cdot \frac{b_s^2 L}{\bar{V}} \cdot \bar{m} \end{pmatrix}$$

Once the $q_j(t)$ is determined, the physical displacements are obtained by the mode summation procedure given in Eq. (3). Note that additional efforts on aerodynamic force transfer between the fluid flow and the structural solver are not needed with current fully coupled FSI approach. The mode shapes given at each grid point are redefined on the cell center point using simple interpolation within the solver. In this way, the aerodynamic force estimated on each cell center of the blade surface mesh are directly used to solve the modal equations given by Eq. (6).

3.2 Implicit Structural Solver

To solve the structural equations with CFD solver [24, 30] in a fully coupled manner, the decoupled structural equations are integrated using the same method as the flow governing equations [17, 19].

$$\begin{aligned}\left(\tfrac{1}{\Delta\tau}I + \tfrac{1.5}{\Delta t}M + K\right)\delta S^{n+1,m+1} \\ = q^{n+1,m+1} - M\tfrac{3S^{n+1,m} - 4S^n + S^{n-1}}{2\Delta t} - KS^{n+1,m}\end{aligned} \tag{8}$$

where n is physical time step and m represents pseudo time step. Within each physical time step, the flow equations and structural equations are solved iteratively via successive pseudo time step until the prescribed convergence criteria are satisfied for both flow and structural solver. After the convergence criteria are reached, the fluid-structural interaction goes to next physical time step.

4 Boundary Conditions

At the fan inlet, the given radial distributions of total pressure, total temperature, swirl angle and pitch angle are

applied and velocity is extrapolated from the computational domain in order to determine the rest of variables. On the blade surface and casing wall a non-slip boundary condition is applied, while on the hub surface the law of the wall is used to avoid an excessively fine mesh in the boundary layer [23]. At the rotor outlet, the static pressure is specified in the spanwise direction. The velocity components are extrapolated from the computational domain and an isentropic relation is used to determine density. If the wall surface is rotating, the wall static pressure is determined by solving the radial equilibrium equation. If the wall surface is stationary, then the static pressure gradient across the wall boundary is set to zero. In addition, the adiabatic condition is used to impose zero heat flux through the wall. To avoid calculation of full annulus rotor, a boundary condition needs to be setup on the circumferential boundaries of a sector of the rotor. The time-shifted phase lag (TSPL) BC suggested by Erods et al. [31] and implemented by the present authors [19] based on the phase periodicity with the period as nodal diameter is applied.

5 Travelling Wave Initial Condition

To impose an initial travelling wave, each blade mode starts to vibrate by a time lag in terms of a given IBPA ($\varphi = 2\pi N_D/N_B$), where N_B is number of blade and N_D is nodal diameter.

$$\delta t_j = \frac{\varphi}{\omega_j} \tag{9}$$

6 The Rotor and Computational Mesh

The transonic rotor studied in this paper is originally studied by Sanders et al. at Honeywell [20]. The test was conducted as a single stage composed of a rotor and stator. In this paper, only the rotor is simulated. The fan used in this study flutters with FTW at 2 nodal diameter (ND). To consider the effect of phase difference on flutter, 2 rotor blade passages are calculated. The IBPA imposed for this rotor is 32.72deg observed from the experiment.

The computational mesh of half annulus with 11 blade passages constructed using a H-O-H mesh topology shown in Fig. 1 is used. The rotor tip clearance is fully modeled using a O-mesh of 201(around blade)×21(blade-to-blade)×9(radial tip clearance), e.g. refer to [23]. For the main mesh, the size of blade passage is 201(around blade)×81(blade-to-blade)×64(radial or blade span). Inlet and outlet duct of the main H-mesh are 21×31×64 respectively. This gives a total main mesh size of 7,136,151 for the half annulus with 11 blade passages. The present mesh shows a good convergence to the choke mass flow, which is about 0.5% lower than the measurement. One blade passage is partitioned into 14 blocks, which gives total 154 blocks for half annulus.

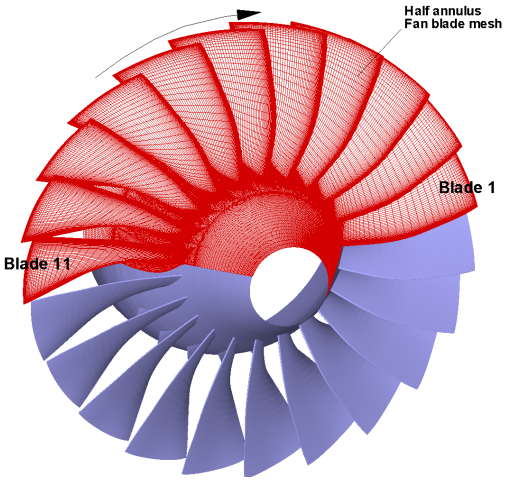

FIGURE 1: Half annulus computational mesh

7 Mode Shape

The first five mode shapes normalized by the generalized mass are used in the current study and the 1st and the 5th mode shapes are displayed in Fig. 2. The blades are modeled as fixed at the rigid body rotor. The first natural frequency is about 430 Hz and the blade passing frequency(BPF) is about 6000 Hz.

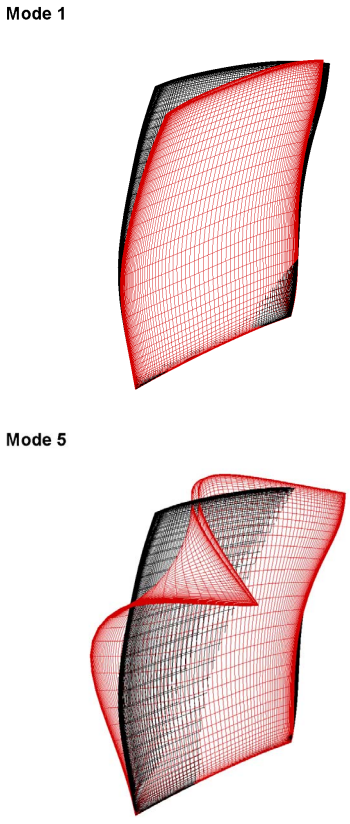

FIGURE 2: Fan blade modal deflections for the 1st and 5th mode

8 Predicted Speedline

The whole speedline from near choke to the mass flow near the flutter is first obtained by increasing the backpressure using the steady state rigid blade simulations. The mass flow near choke condition is predicted by about 0.5% lower than the measurement. Overall the predicted speedline is in good agreement near the flutter boundary as shown in Fig. 3. The peak efficiency of the transonic fan predicted by the RANS appears between point A and B. The fan rotor runs with a little efficiency decrease after point B. The fully coupled FSI simulations including point A, B, C, D and E are started from the converged steady state solutions. A dimensionless time step of 0.001 is used, i.e. roughly 300 time steps per cycle for the 1st mode. For the unsteady simulations the residual is dropped up to the level of around 1e-9 by two orders of magnitude reduction within each physical time step, which needs approximately 10 to 20 pseudo iterations.

The flutter of the transonic fan occurs between point D and E at the blade 1st mode, which agrees with the experiment. A rotating stall signal such as a steep pressure drop with the mass flow breakdown is not identified near the flutter region as presented in Fig. 4. The mass flow oscillates in a phase-locked manner during the flutter, which indicates no rotating stall.

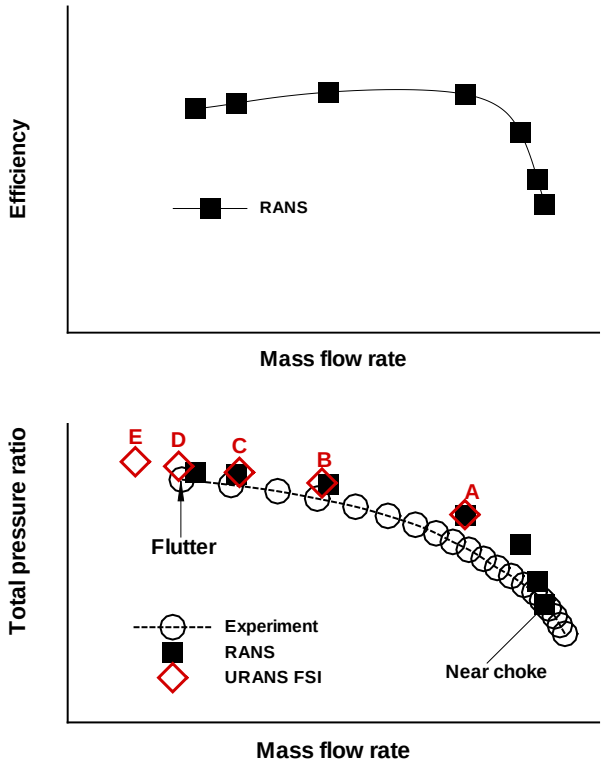

FIGURE 3: Predicted fan speedline and adiabatic efficiency

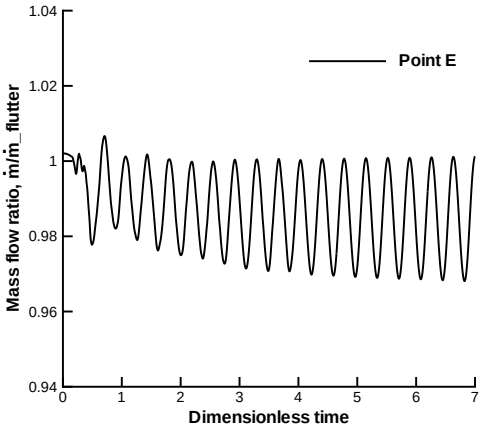

FIGURE 4: Time history of the mass flow ratio($\frac{\dot{m}}{\dot{m}_{flutter}}$), where $\dot{m}_{flutter}$ is the measured mass flow at the flutter

9 Unsteady Fully Coupled FSI Simulations

To investigate the flutter, the fully coupled FSI simulations are performed at point A, B, C, D and E with a forward travelling wave at 2 nodal diameter. A structural damping ($\zeta_{structural}$), which is unknown and typically very small, is enforced as zero to obtain pure aerodynamic damping ($\zeta_{aero} = \zeta_{total} - \zeta_{structural}$) from the unsteady FSI simulations. Each blade eigenmode is initially perturbed using a small modal velocity $\dot{q}_j$. Note that this simulations use the blade responses from the fully coupled FSI to identify flutter. The blade responses over 10 cycles are used to see if the blade vibration is damped out or not, and for the calculation of total damping ζ_{total} [32]. Positive aerodynamic damping means stable and damped vibration whereas flutter occurs with negative aerodynamic damping [9].

The predicted aerodynamic damping coefficients from the fully coupled FSI simulations at point A to E are plotted in Fig. 5. At point E, the flutter occurs with negative aerodynamic damping. The predicted aerodynamic damping shows that the flutter boundary exist between point D and E, which matches well the experiment. The blade response at point A has lower aerodynamic damping than point B, which may be the point A is closer to the choking. Note that no flutter near choke is identified in the transonic fan experiment.

Fig. 6 and Fig. 7 show the predicted 1st mode displacements of blade 11 (solid line) and blade 6 (dashed line) at point A, B, C and D, E respectively. Obviously the flutter boundary exits between point D and E because the blade vibration at point D is near neutral response and that of point E is flutter with increasing response in time. The other blades also show the similar to blade 11. The only difference is the phase angle difference due to the forward travelling wave at 2 nodal diameter. Note that X_0 is about 0.00022 in the aerodynamic damping function and ω_n is the 1st mode blade natural frequency of about 430 Hz.

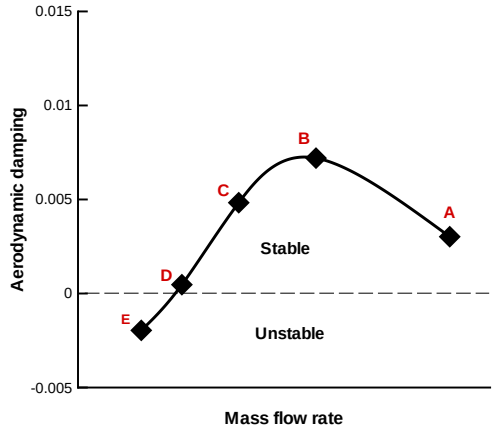

FIGURE 5: Predicted aerodynamic damping, ζ_a indicating flutter at point E due to the negative damping

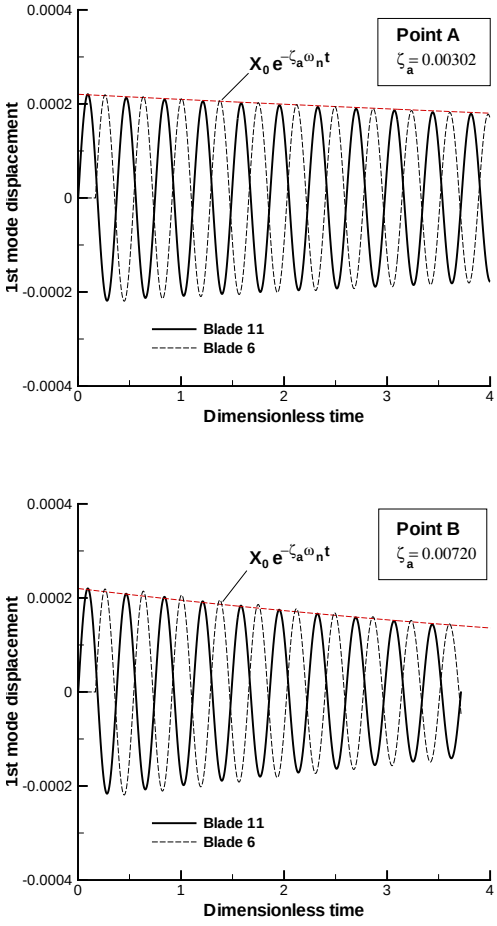

FIGURE 6: Predicted 1st mode displacements and aerodynamic damping ζ_a for blade 11 (solid line) and blade 6 (dashed line) at point A (top) and B (bottom)

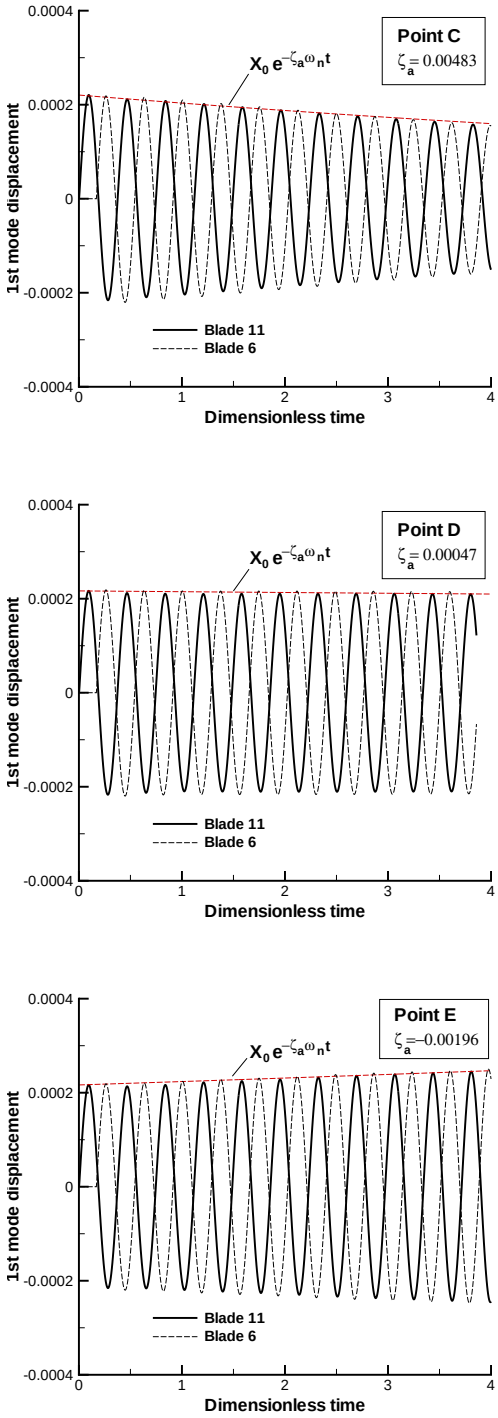

FIGURE 7: Predicted 1st mode displacements and aerodynamic damping ζ_a for blade 11 (solid line) and blade 6 (dashed line) at point C (top), D (middle) and E (bottom)

Fig. 8 shows the 1st, 2nd, and 3rd mode displacements of blade 11 during the flutter (point E). Obviously the flutter occurs with a diverging response at the 1st mode, whereas the displacements for 2nd and 3rd mode are being damped out. Note that the modal displacements for the 4th and 5th mode also decay out. Fig. 9 shows the estimated aerodynamic damping coefficient for mode 1, 2 and 3 at point E. The 2nd and 3rd mode are stable without flutter.

In Fig. 10, the 1st mode displacements for the blades contained in the half annulus sector are plotted. The propagation of a travelling wave in the same direction of the rotor rotation, which is a forward travelling wave (FTW), is clearly captured with a constant phase angle difference by 2 nodal diameter. The effect of nodal diameter (or inter blade phase angle) on the flutter is not included in this study.

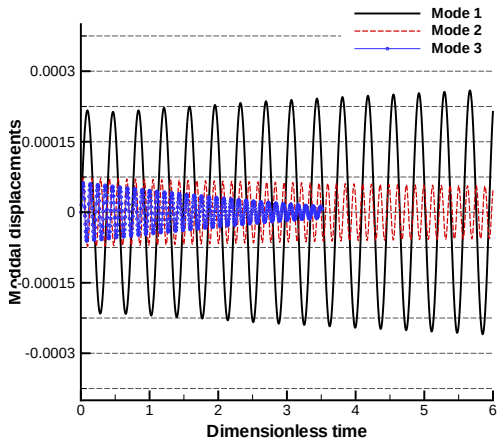

FIGURE 8: Predicted 1st, 2nd, and 3rd mode displacements of blade 11 during the flutter (Point E)

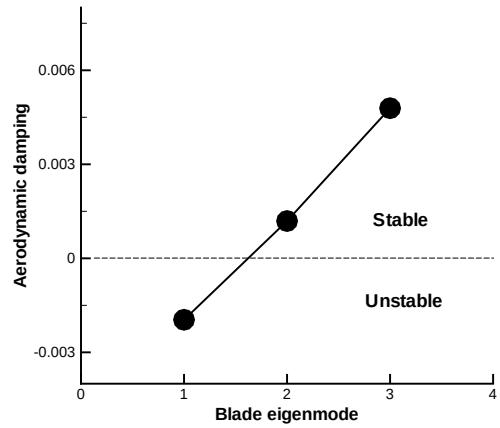

FIGURE 9: Predicted modal aerodynamic damping ζ_a at point E

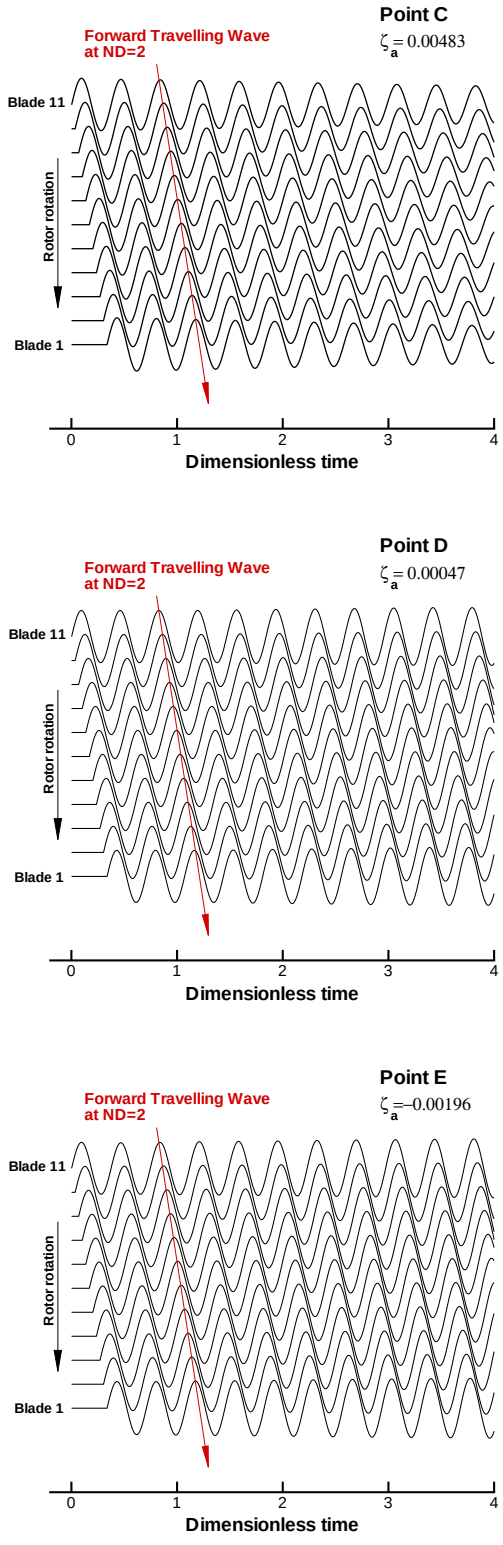

FIGURE 10: Predicted 1st mode displacements with a forward travelling wave at 2 nodal diameter

10 The Mechanism of the Fan Flutter

As mentioned in the introduction, it has been demonstrated that the shock waves have a significant impact on a transonic fan/compressor flutter [4–9]. The shock structure for the transonic fan at a stable operation (point B) is illustrated in Fig. 11. The strong normal shock detached from the rotor leading edge is captured at 85% blade span (top). There is a thick boundary layer on the suction surface after the shock/boundary layer interaction. The shock structure at the tip span (bottom) is more complex compared to 85% span due to the interaction of the shock with tip leakage flow and the boundary layer. The fact is that this shock moves on the suction surface according to the backpressure levels as presented in Fig. 12. The shock over 70% span moves further upstream as the backpressure level increases. Note that the normalized backpressure at point B, D, E is 4.3, 4.46, 4.51 respectively. In this study, the shock movement is shown to significantly increase the unsteadiness in the blade passage and to create the serious blockage in the vicinity of the blade tip due to the interaction with the tip leakage vortex.

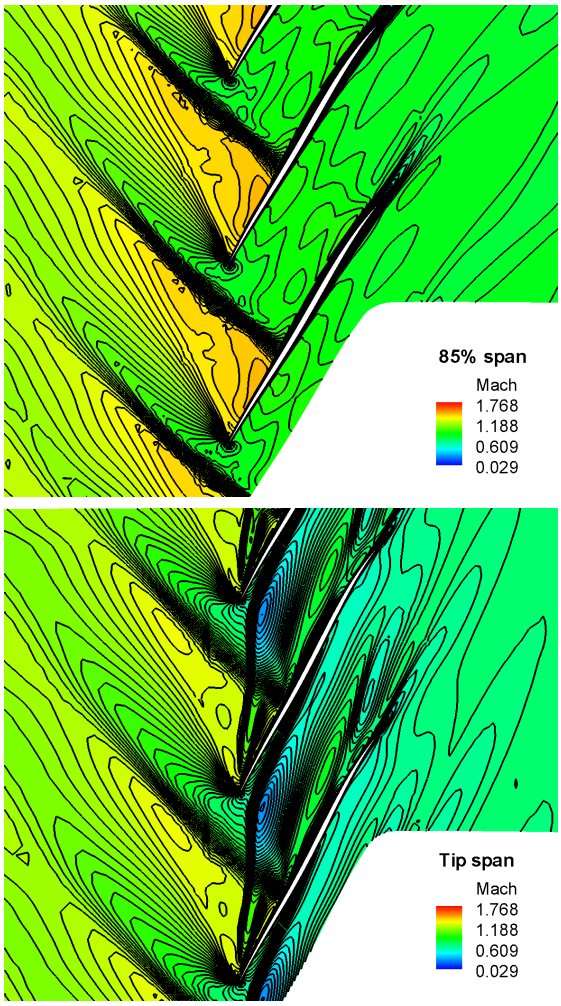

FIGURE 11: Shock structure of the transonic fan at a stable operation (point B); 85% span (top), tip span(bottom)

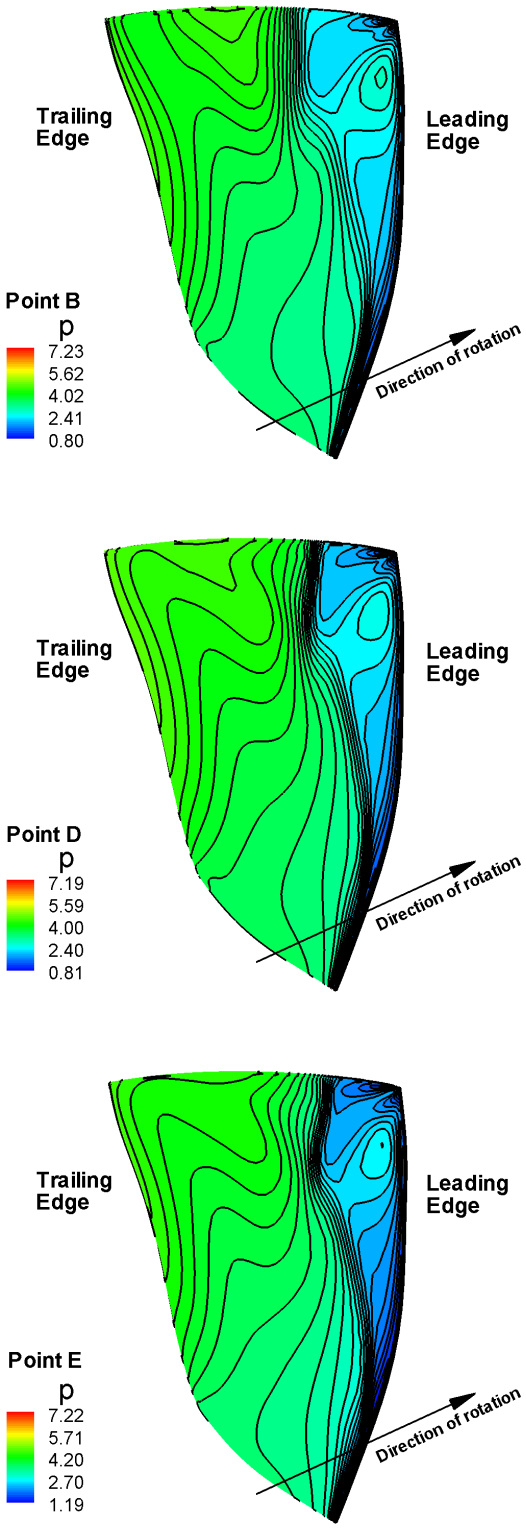

FIGURE 12: Variations in the blade suction surface normalized static pressure P at point B (top), D (middle) and E (bottom)

Fig. 13 shows the pressure coefficients (C_p) of the tip meridional plane at point B, C, D and E. The dimensionless distance of zero is near the blade passage inlet, and 0.09 is near the blade passage outlet. The shock at point B indicated by the sharp pressure drop goes to the upstream of the blade passage as the back pressure increases. The position of the shock at point B, D, E near zero C_p is about 0.0333, 0.0283, 0.0257 respectively. The normalized meridional distance over the tip passage is about 0.0942. Therefore, the flutter of the transonic fan occurs when the shock is located below 30% tip meridional chord because the predicted aerodynamic damping at point D (30% meridional chord) is nearly zero and negative at point E (27% meridional chord).

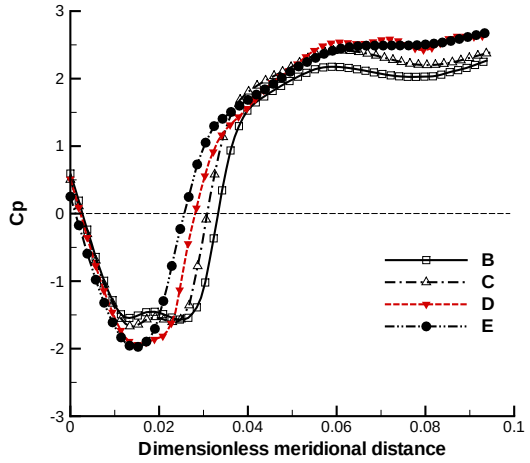

FIGURE 13: Changes in the pressure coefficients (C_p) at the meridional plane of the blade tip section

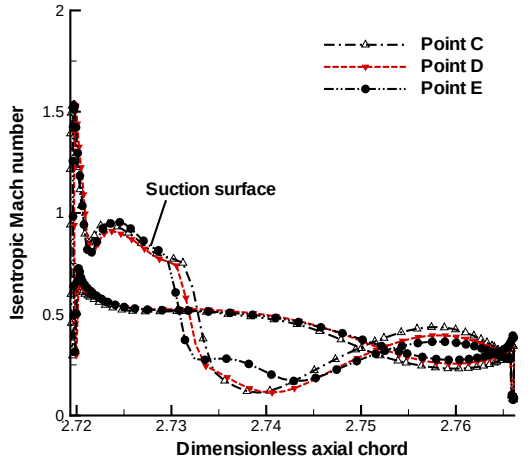

FIGURE 14: Changes in the blade surface isentropic Mach number at about 90% span

Fig. 14 shows the blade surface isentropic Mach number at 90% span at point C, D and E. There are no shocks on the pressure surface since the shocks are detached from the blade passage. Again, the flutter is sensitive to the location of the detached shock on the suction. The flutter appears with the negative aerodynamic damping below point D. A recent experimental study [33] on the unsteady flow and shock motion of a transonic low aspect ratio fan, which is similar to the fan used in this study, showed that the coherent unsteadiness as a result of the shock movement is increased significantly when the shock system becomes detached from the leading edge and extends out from the blade passage due to the interaction between the clearance flow and the shock. The shock system observed in this fan is a detached normal shock even at point B, e.g. see Fig. 11.

Tip leakage vortex interactions with the detached shock at point B (top) and E (bottom) captured just below the blade tip section are illustrated in Fig. 15. The shock/tip leakage vortex interaction at point E (flutter) occurs at further upstream, which introduces very low Mach number region and more unsteadiness behind the shock. It is clear that the blockage behind the shock during the flutter is larger than point B. The enlarged blockage in front of the blade passage can disturb the incoming flow to the blade and can introduce an aerodynamic instability due to higher incidence to the blade. It is shown by the transonic compressor flutter test [34] that the flow incidence angle with respect to relative Mach number at the blade leading edge is the key aerodynamic parameter for the flow field characteristics at the flutter boundaries. Another explanation for this flutter is that the shock system occurring further upstream of the blade section can increase the pitching momentum over the dynamic equilibrium condition, e.g. refer to [9].

Fig. 16 shows instantaneous Mach number variations near the blade tip passage inlet before/after the flutter. 0 % blade pitch denotes the passage inlet near suction side and 100% the passage inlet near pressure side. The tip flow roughly above 60% blade pitch is subsonic before flutter (point B and D), whereas the subsonic flow field is extended by 20% toward blade suction side with flutter (point E) due to the strong blockage created by the shock/tip leakage vortex interaction.

The numerical probes are placed to acquire unsteady static pressure. The probe p1 is located around the detached normal shock on the suction surface and p2 is located near the rotor leading edge on the pressure side. Fig.17 shows the travelling pressure wave at p1 (top) and p2 (bottom) at point E (flutter). Note that the same scale is used to plot the pressure wave at p1 and p2 in Fig.17. Both waves are propagating in the same direction of the rotor rotation (FTW) with increasing amplitude. The pressure wave at p2 shows larger fluctuations than at p1 during the flutter because the flow field behind the shock/tip leakage vortex interaction becomes more unstable than near the shock area due to the larger blockage with very low velocity. In addition, there is a small phase angle difference between the pressure wave at p1 (on the suction surface) and at p2 (on the pressure side) because the wave propagates in the direction of the rotor from

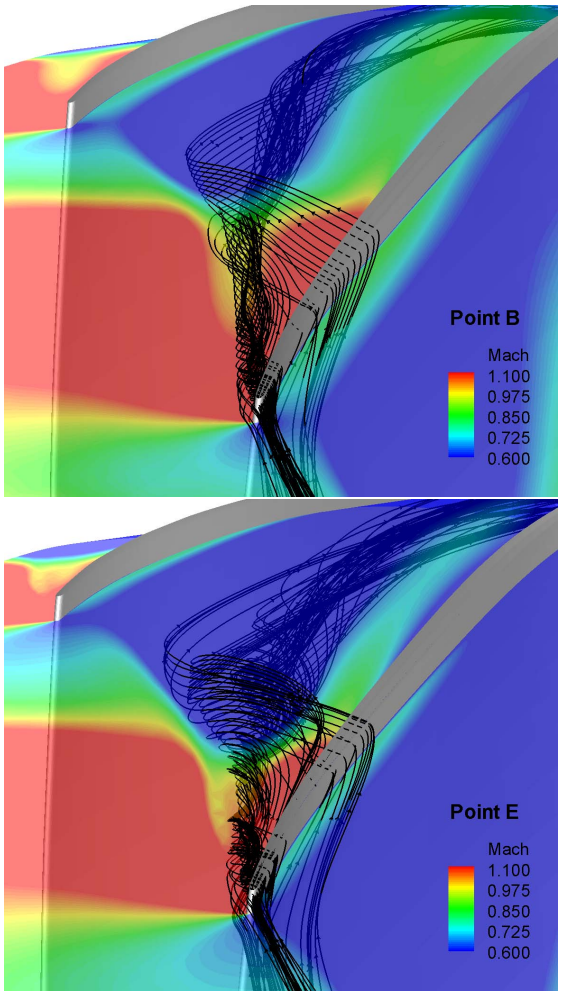

FIGURE 15: Instantaneous tip clearance vortex trajectories with Mach number contour at point B (top) and E (bottom)

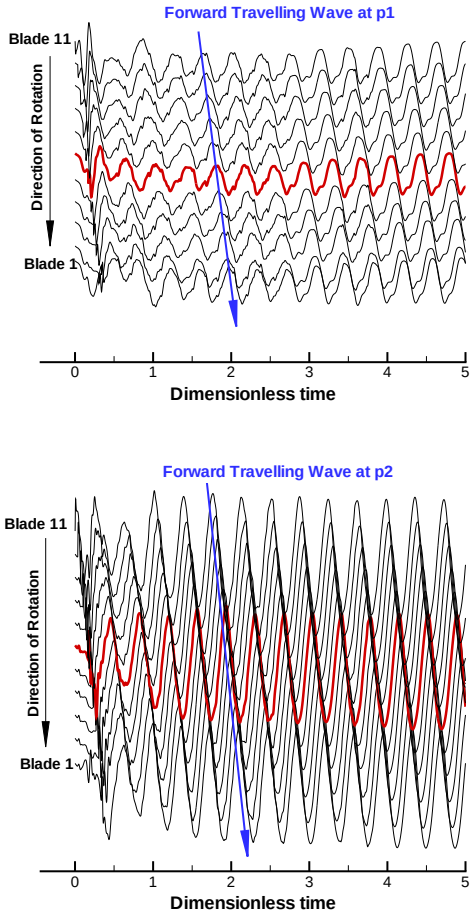

FIGURE 17: Forward travelling pressure wave at probe p1 (top) and p2 (bottom) during the flutter (point E)

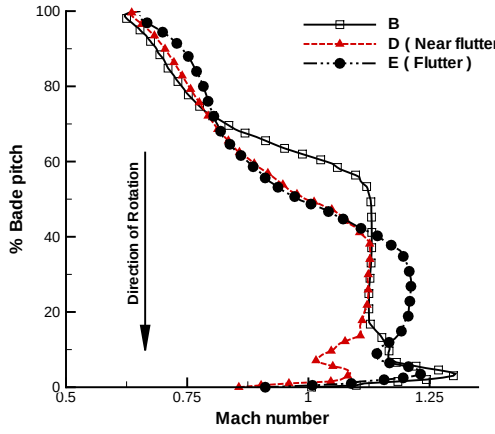

FIGURE 16: Instant Mach number variations near the blade tip passage inlet

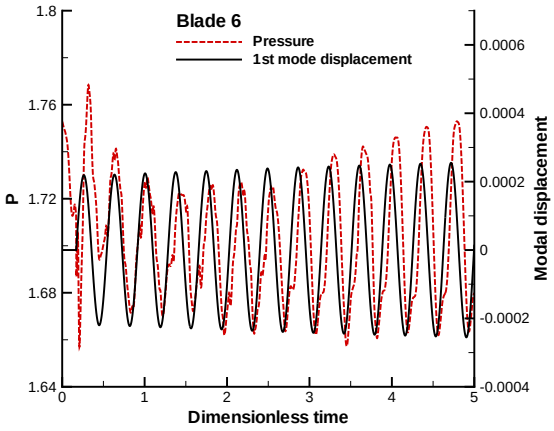

FIGURE 18: Normalized static pressure signal near the normal shock versus 1st mode displacement during the flutter (point E)

the pressure side to the suction side.

In Fig. 18, the unsteady pressure acquired near the shock is compared to the 1st mode blade displacement at point E. After about two transitional periods, the pressure becomes periodic with increasing oscillation and shows a small phase difference with the blade displacement during the flutter. It is observed that the period of the pressure signal is about the same as that of the blade vibration. The predicted frequency for the pressure signal near the strong detached shock matches the flutter frequency at the 1 st mode as presented in Fig. 19. The shock instability appears to be the root cause of the transonic fan flutter observed in this study.

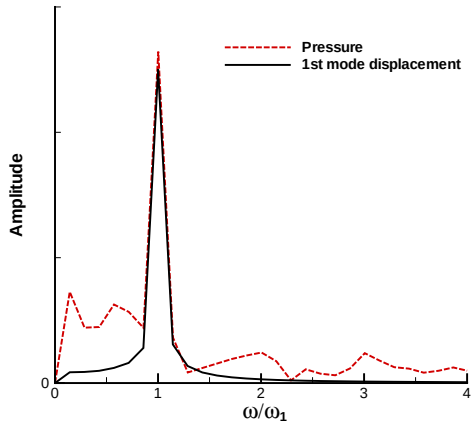

FIGURE 19: Predicted frequencies for the pressure signal near the normal shock and for the 1st mode displacement during the flutter (point E), where ω_1 is the 1st mode natural frequency of the blade

11 Conclusions

Numerical investigations for a low aspect ratio transonic fan using a fully coupled fluid/structure interaction method are conducted to identify the possible causes of the flutter. A forward travelling wave at 2 nodal diameter is modeled using a half annulus sector with a time shifted phase lag BC at the lower/upper circumferential boundaries. The 5th order WENO scheme with a low diffusion Riemann solver is employed to accurately resolve the fluid/structure interaction of the fluttering transonic fan blades.

The present flutter simulations with a travelling wave show that the flutter of the transonic fan is a shock driven instability at the blade 1st mode before the stall, and the predicted flutter boundary is in good agreement with the experiment. It is shown that the stability of the blade motion relies on the normal shock position on the suction surface. When the shock at the tip section is located roughly below 30% blade chord, the flutter of the transonic fan occurs due to the larger blockage created by the interaction of the detached normal shock with tip leakage vortex.

Acknowledgement

We thank Honeywell for approving publishing the results. The grants support from AFRL and the industrial partners of GUIde Consortium, 10-AFRL-1024 and 09-GUIDE-1010, are acknowledged. The numerical simulations are conducted at the Center for Computational Sciences at the University of Miami and Air Force Research Lab DoD Supercomputing Resource Centers.

REFERENCES

[1] M. Baumgartner, F. Kameier, and J. Hourmouziadis, "Non-Engine Order Blade Vibration in a High Pressure Compressor." ISABE, Twelfth International Symposium on Airbreathing Engines, Melbourne, Australia, 10-15, 1995.

[2] F. Sisto, S. Thangam, and A. Abdel-Rahim, "Computational Prediction of Stall Flutter in Cascade Airfoils," *AIAA Journal*, vol. 29, pp. 1161–1167, 1991.

[3] A.V. Srinivasan, "Flutter and Resonant Vibration Characteristics of Engine Blades." ASME 97-GT-533, October 1997.

[4] D.G. Halliwell, "Fan Supersonic Flutter: Prediction and Test Analysis." Aeronautical Research Councel R.&M. No. 3789, 1977.

[5] K. Isomura, and M.B. Giles, "A Numerical Study of Flutter in a Transonic Fan," *Journal of Turbomachinery*, vol. 120, pp. 500–507, 1998.

[6] P. Vasanthakumar, "Computation of Aerodynamic Damping for Flutter Analysis of a Transonic Fan." GT2011-46597, 2011.

[7] J.W. Chew, R.J. Hamby, J.G. Marshall, and M. Vahdati, " Part Speed Flutter of Transonic Fan." RTO AVT Symposium on Design Principles and Methods for Aircraft Gas Turbine Engines, Toulouse, France, May 1998, 1998.

[8] M. Vahdati, G. Simpson, and M. Imregun, "Mechanisms for Wide-Chord Fan Blade Flutter," *Journal of Turbomachinery*, vol. 133, pp. 041029–1–041029–7, 2011.

[9] R. Srivastava, and T.G. Keith Jr., "Influence of Shock Wave on Turbomachinery Blade Row Flutter," *Journal of Propulsion and Power*, vol. 21, pp. 167–174, 2005.

[10] R. Kamakoti, and W. Shyy, "Fluid-Structure Interaction for Aeroelastic Applications," *Progress in Aerospace Sciences*, vol. 40, pp. 535–558, 2004.

[11] V. Gnesin, and R. Rzadkowski, "A Coupled Fluid-Structure Analysis for 3-D Inviscid Flutter of IV Standard Configuration," *Journal of Sound and Vibration*, vol. 251, pp. 315–327, 2002.

[12] H. Doi, and J.J. Alonso, "Fluid/Structure Coupled Aeroelastic Computations for Transonic Flows in Turbomachinery." GT2002-30313,Proceedings of ASME Turbo Expo 2002, 2002.

[13] V. Carstens, R. Kemme, and S. Schmitt, "Coupled Simulation of Flow-Structrue Interaction in Turbomachinery," *Aerospace Science and Technology*, vol. 7, pp. 298–306, June 2003.

[14] A.I. Sayma, M.V. Vahdati, and M. Imregun, "Turbine Forced Response Prediction Using an Integrated Non-Linear Analysis," *Proceedings of the Institution of Mechanical Engineers, Part K: Journal of Multi-body Dynamics*, vol. 214, pp. 45–60, 2000.

[15] R. Srivastava, and T. S. R. Reddy, "Comparative Study of Coupled-Mode Flutter-Analysis Methods for Fan Configurations," *Journal of Propulsion and Power*, vol. 15, pp. 447–453, May-June 1999.

[16] H.-S. Im, X.-Y. Chen, and G.-C. Zha, " Detached Eddy Simulation of Transonic Rotor Stall Flutter Using a Fully Coupled Fluid-Structure Interaction." ASME GT2011-45437, ASME Turbo Expo 2011, Vancouver, Canada, June 2011, 2011.

[17] X.Y. Chen, G.-C. Zha, M.-T. Yang, "Numerical Simulation of 3-D Wing Flutter with Fully Coupled Fluid-Structural Interaction," *Journal of Computers & Fluids*, vol. 36, pp. 856–867, 2007, doi:10.1016/j.compfluid.2006.08.005.

[18] H. Im, X. Chen, and G. Zha, "Prediction of a Supersonic Flutter Boundary Using a High Fidelity Delayed Detached Eddy Simulation." 50th AIAA Aerospace Sciences Meeting, Nashville, Tennessee, Jan. 2012, 2012.

[19] H.S. Im, and G.C. Zha, "Simulation of Non-Synchronous Blade Vibration of an Axial Compressor Using a Fully Coupled Fluid/Strcuture Interaction." ASME GT2012-68150, 2012.

[20] A.J. Sanders, K.K. Hassan, and D.C. Rabe, "Experimental and Numerical Study of Stall Flutter in a Transonic Low-Aspect Ratio Fan Blisk," *Journal of Turbomachinery*, vol. 126, pp. 166–174, 2004.

[21] F. Lane, "System Mode Shapes in the Flutter of Compressor Blade Rows," *Journal of the Aeronautical Science*, vol. 23, pp. 54–66, 1956.

[22] P.R. Spalart, and S.R. Allmaras, "A One-equation Turbulence Model for Aerodynamic Flows." AIAA-92-0439, 1992.

[23] H.S. Im, X.Y. Chen, and G.C. Zha, "Detached Eddy Simulation of Stall Inception for a Full Annulus Transonic Rotor," *Journal of Propulsion and Power*, vol. 28 (No. 4), pp. 782–798, doi: 10.2514/1.58970, 2012.

[24] G.C. Zha, Y.Q. Shen, and B.Y. Wang, "An Improved Low Diffusion E-CUSP Upwind Scheme ," *Journal of Computer and Fluids*, vol. 48, pp. 214–220, 2011, doi:10.1016/j.compfluid.2011.03.012.

[25] Y.Q. Shen, G.C. Zha, and B.Y. Wang, "Improvement of Stability and Accuracy of Implicit WENO Scheme," *AIAA Journal*, vol. 47, pp. 331–334, DOI:10.2514/1.37697, 2009.

[26] Y.Q. Shen, B.Y. Wang, and G.C. Zha, "Implicit WENO Scheme and High Order Viscous Formulas for Compressible Flows ." AIAA Paper 2007-4431, 2007.

[27] B. Wang, Z. Hu, and G. Zha, "A General Sub-Domain Boundary Mapping Procedure For Structured Grid CFD Parallel Computation," *AIAA Journal of Aerospace Computing, Information, and Communication*, vol. 5, pp. 425–447, 2008.

[28] B. Gruber, and V. Carstens, "The impact of Viscous Effects on the Aerodynamic Damping of Vibrating Transonic Compressor Blades - A Numerical Study," *Journal of Turbomachinery*, vol. 123, pp. 409–417, 2001.

[29] H. Im, "High Fidelity Simulation of Non-Synchronous Vibration for Aircraft Engine Fan/Compressor." PhD Dissertation, University of Miami, 2012.

[30] Zha, G.C., Shen, Y.Q., and Wang, B.Y., "Calculation of Transonic Flows Using WENO Method with a Low Diffusion E-CUSP Upwind Scheme." AIAA Paper 2008-0745, 46th AIAA Aerospace Sciences Meeting, Reno, NV, Jan. 2008.

[31] J.I. Erods, E. Alzner, and W. McNally, "Numerical Solution of Periodic Transonic Flow Through a Fan Stage," *AIAA Journal*, vol. 15, pp. 1559–68, Nov. 2004.

[32] D. Gottfried, and S. Fleeter, "Aerodynamic Damping Predictions in Turbomachines Using a Coupled Fluid-Structure Model," *AIAA Journal of Propulsion and Power*, vol. 21, pp. 327–334, 2005.

[33] W. W. Copenhaver, and S. L. Puterbaugh, "unsteady Flow and Shock Motion in a Transonic Compressor Rlotor," *AIAA Journal of Propulsion and Power*, vol. 13, pp. 17–23, 1997.

[34] R. R. Jutras, M. J. Stallonet, and H.R.Bankhead, "Experimental Investigation of Flutter in Midstage Compressor Designs," *Journal of Aircraft*, vol. 18, pp. 874–880, Oct. 1981.